Bureau of Mines Report of Investigations/1987

Size Scaling of Gas Explosions: Bruceton Experimental Mine Versus the Lake Lynn Mine

By M. J. Sapko, E. S. Weiss, and R. W. Watson

UNITED STATES DEPARTMENT OF THE INTERIOR

Report of Investigations 9136

Size Scaling of Gas Explosions: Bruceton Experimental Mine Versus the Lake Lynn Mine

By M. J. Sapko, E. S. Weiss, and R. W. Watson

UNITED STATES DEPARTMENT OF THE INTERIOR
Donald Paul Hodel, Secretary

BUREAU OF MINES
David S. Brown, Acting Director

Library of Congress Cataloging in Publication Data:

Sapko, M. J.
Size scaling of gas explosions.

(Report of investigations ; 9136)

Bibliography: p. **23**.

Supt. of Docs. no.: I 28:23: 9136.

1. Mine explosions. 2. Coal mines and mining–Dust control. 3. Coal mines and mining–Fires and fire prevention. I. Weiss, E. S. (Eric S.). II. Watson, Richard William, 1927–____. III. Title. IV. Series: Report of investigations (United States. Bureau of Mines) ; 9136.

TN23.U43 [TN313] 622 s [622'.8] 87-600189

CONTENTS

ILLUSTRATIONS

ILLUSTRATIONS--Continued

TABLES

UNIT OF MEASURE ABBREVIATIONS USED IN THIS REPORT

atm	atmosphere	$lbf \cdot s/ft^2$	pound (force) second per square foot
Btu	British thermal unit	mm	millimeter
$cal/cm^2 \cdot s$	calorie per square centimeter second	mV	millivolt
°F	degree Fahrenheit	pct	percent
ft	foot	psi	pound (force) per square inch
ft^2	square foot	psia	pound (force) per square inch, absolute
ft^3/min	cubic foot per minute	psig	pound (force) per square inch, gauge
ft/s	foot per second	s	second
ft/s^2	foot per square second	st	short ton
h	hour	V	volt
in	inch		
in Hg	inch of mercury		

SIZE SCALING OF GAS EXPLOSIONS: BRUCETON EXPERIMENTAL MINE VERSUS THE LAKE LYNN MINE

By M. J. Sapko[1], E. S. Weiss,[2] and R. W. Watson[3]

ABSTRACT

Single-entry gas-explosion characteristics for the Bruceton Experimental Mine (BEM) are compared to those occurring in the larger geometries of the new Lake Lynn Mine (LLM) within the Lake Lynn Laboratory (LLL). (All three are Bureau of Mines facilities.) Scale factors and boundary conditions for the BEM and the larger entries of the LLM are reviewed in some detail using representative data for pressure, flame, and wind velocity in the two mines. Measured pressure histories for gas explosions at the BEM are compared with data for comparable explosions in the larger cross section of the LLM.

The time evolution for flame-front displacement can be characterized by a general expression that relates gas concentration and length of flammable volume. The course of the explosion development and its destructive power are dependent upon the development of turbulence in the unburned flammable mixture into which the flame propagates. The results of this study indicated that pressure profiles in the larger cross section are maintained to much larger distances even though the flame front is accelerated less rapidly in a comparable entry length of smaller flammable volume.

[1]Supervisory chemical engineer.
[2]Mining engineer.
[3]Research supervisor.
Pittsburgh Research Center, Bureau of Mines, Pittsburgh, PA.

INTRODUCTION

Coal dust explosions are a constant hazard in underground coal mining operations. Such disasters are usually started by the ignition of a methane (CH_4)-air pocket, which may develop a sufficient heat and aerodynamic disturbance to pick up, disperse, and ignite any accumulated coal dust. Thus, the ignition of coal dust explosions by the use of a premixed CH_4-air pocket has become a routine experimental test procedure. Once initiated, a self-sustained dust explosion can propagate over large distances in the mine, causing injuries and fatalities to miners and extensive destruction of equipment (1-2).[4] The Bureau of Mines has been conducting full-scale mine explosion research in the BEM (Bruceton, PA) for many years. Pressure and flame travel relationships have been mapped out under a variety of experimental conditions in the 6-ft-high by 9-ft-wide BEM. Completion of the LLM, as described by Mattes (3), provided the opportunity for similar measurements in entries having approximately twice the cross-sectional area of the BEM. This report describes these measurements and compares results of gas explosion tests in the two facilities.

NEW EXPLOSION TEST FACILITY

The LLL occupies approximately 400 acres and is located 15 miles north of Morgantown, WV. The LLM consists of large entries developed in the mid-1960's as part of a commercial limestone mining operation. It was further developed in 1980-81 by constructing new entries totaling 7,500 ft in length that are 20 ft wide by 6.8 ft high. The newly developed entries are used for explosion tests. Figure 1 shows a plan view of the underground entries of the LLM. A plan view of the older BEM is shown in figure 2. Figure 3 compares the relative entry sizes of the BEM and the LLM.

The new underground workings at the LLM include two movable explosion-proof bulkheads. These bulkheads, which weigh 67 st each, are constructed of concrete and steel and can be positioned anywhere from fully retracted to fully blocking the entry. Their positions are indicated

[4]Underlined numbers in parentheses refer to items in the list of references at the end of this report.

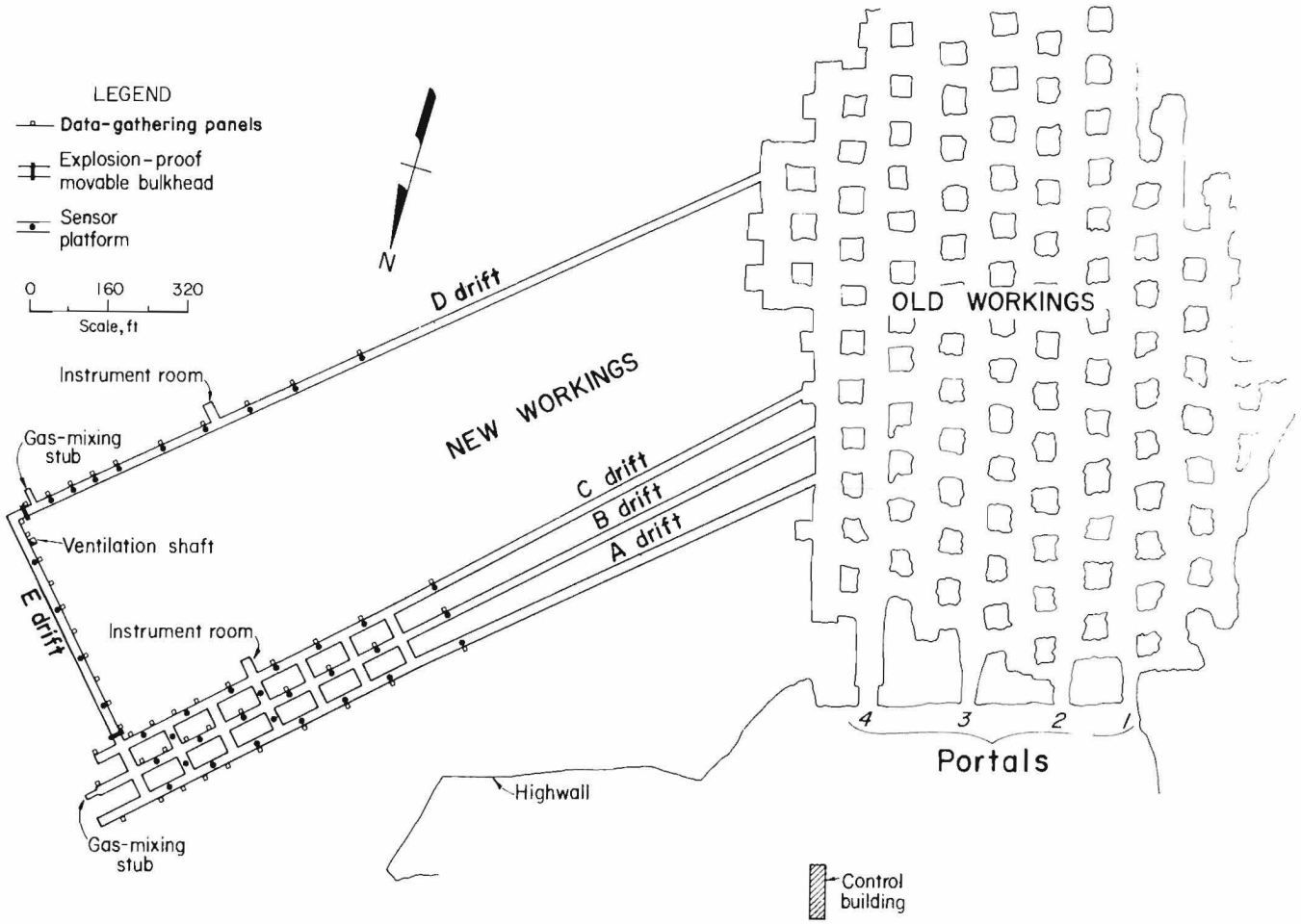

FIGURE 1.—Plan view of LLM underground entries showing location of data-gathering panels.

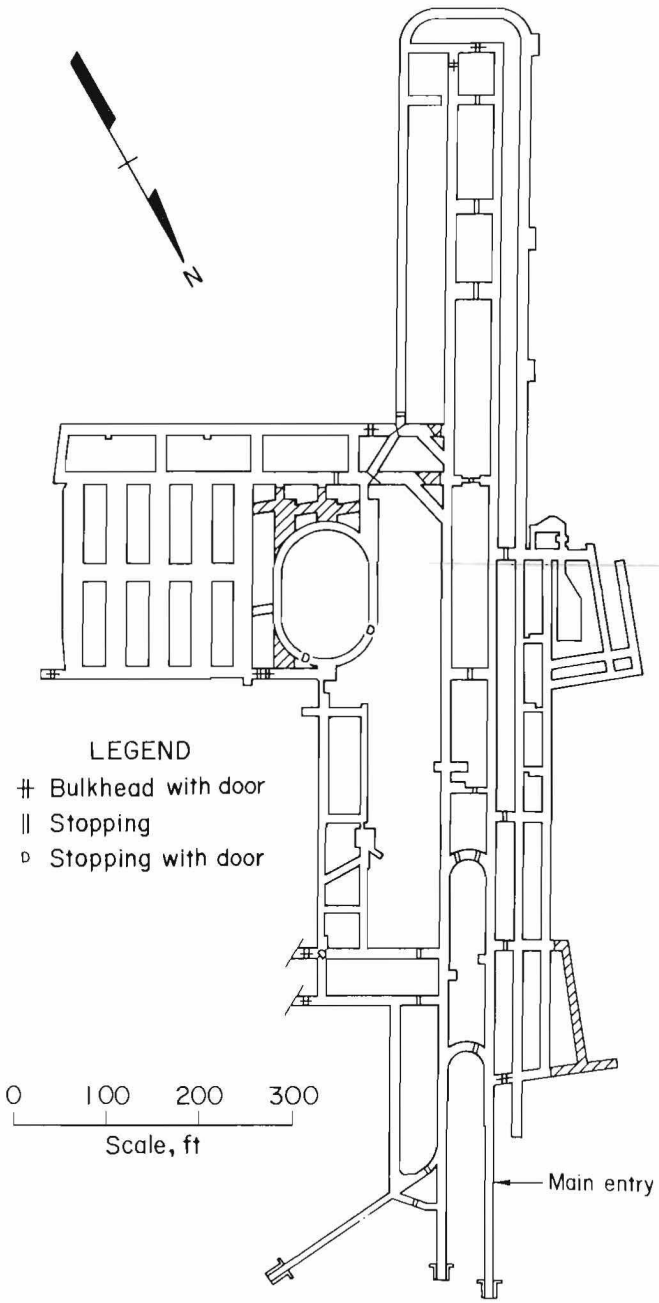

FIGURE 2.—Plan view of BEM showing main entry where explosion tests were conducted.

in Figure 1. By selectively opening or closing these bulkheads, four different underground explosion configurations can be realized. The different configurations are single entry (D drift), triple entry (A, B, and C drifts), longwall face with single entry (E and D drifts), and longwall face with triple entry (E, A, B, and C drifts).

There are two gas-mixing regions (stubs) within the LLM's new workings: one at the head of B drift and the other near the explosion-proof bulkhead in D drift. These stubs provide for the remotely controlled release of flammable gas into various polyethylene-bounded containment zones (gas zones). They can also be used for CH_4 roof-layer studies. Once the flammable gas is released into a contained zone, the gas can be intimately mixed with the contained air by a floor-mounted, explosion-proof booster fan with a capacity of 3,500 ft^3/min. A tube-bundle analysis system (4-5) is used to determine the initial CH_4 concentration in the confined zone, its uniformity, and the postcombustion CO_2 concentration.

Located throughout A, B, C, D, and E drifts are 50 data-gathering panels, as shown in figure 1. Standard sensors within each data-gathering panel include one static pressure transducer and one flame sensor. Control signals are fed from the data-gathering panels to instruments mounted on retractable sensor platforms located in the center of the entries at 38 sites. Photographs of a typical data-gathering panel and sensor platform are shown in figures 4 and 5. When extended, the sensor platform provides a 1-ft^2 horizontal working surface upon which to locate hardware for midstream measurements. The hardware can consist of a camera (as shown) or dust-concentration, wind-velocity, or other sensors.

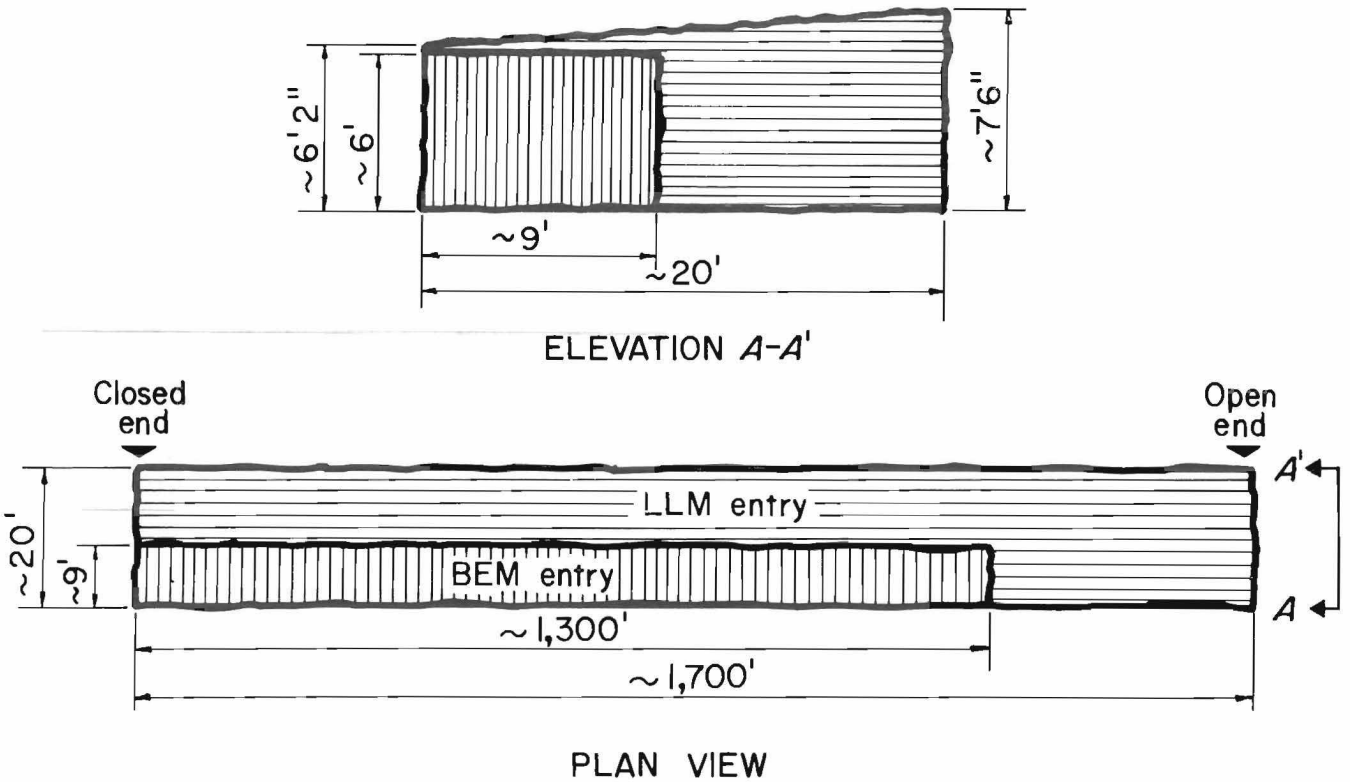

FIGURE 3.—Comparison of entry sizes for BEM and LLM.

DATA-ACQUISITION SYSTEM

The LLL is equipped with a computer-controlled data-acquisition system. This system is capable of collecting and storing 132 input channels of data. During a typical 5-s explosion interval, 3,125,000 data points are stored at a resolution of 5 mV. Within 1 h after an explosion test, the computer produces composite plots of various variables measured during the test.

EXPERIMENTAL PROCEDURE

The gas explosion tests to be reported in this paper were confined in the D drift at the LLM. This 1,664-ft-long entry was sealed off by closing the movable bulkhead. As shown in figure 1, this door, when closed, acts as the closed end or face for a single-entry mine. Gas zones were confined between this bulkhead face and a polyethylene diaphragm, which could be placed at different distances from the face (12, 27, and 40 ft). Flamable gas was injected into the zone and mixed thoroughly with the air and sampled at four points from within the zone to determine CH_4 content and mixture uniformity. Ignition of the gas zones was achieved with one or more electric matches placed at midheight

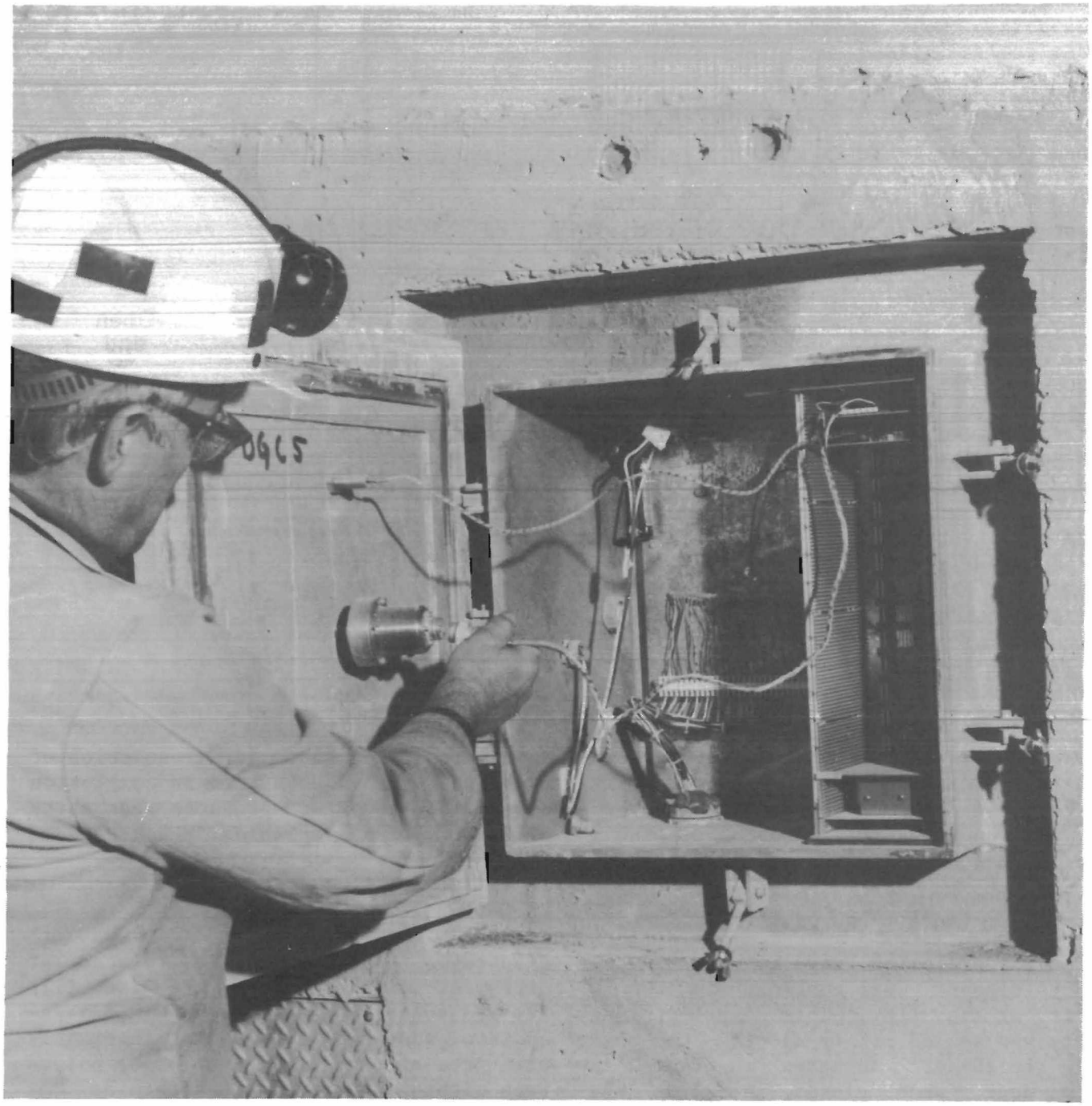

FIGURE 4.—Typical data-gathering panel showing instrumentation and electronics.

FIGURE 5.—Retractable sensor platform with high-speed camera in D-drift.

and 0.5 ft from the face. The single entry is equipped with static-pressure transducers (0 to 100 psia), flame sensors, heat-flux gauges, bidirectional velocity probes, and a 16-mm high-speed movie camera. Analog signals from the sensors are fed back to the control building, to a bank of high-speed oscillograph recorders, and then to the data-acquisition system.

The flamable gas used in the BEM comes from a nearby gas well; whereas, at LLM, the gas is supplied from a transmission line. Analyses of both gas sources are shown in table 1. As shown, the BEM well gas has a higher hydrocarbon value than the LLM gas and a slightly higher heating value per cubic foot of gas. A stoichiometric mixture of the natural gas (NG) at BEM is 8.9 pct, as compared with 9.48 pct for pure CH_4.

TABLE 1. - Analyses of LLM and BEM test gases, percent

Component	LLM	BEM
Methane (CH_4).....	97.8	91.5
Ethane (C_2H_6).....	1.4	4.7
Propane (C_3H_8).....	.04	1.6
Butane (C_4H_{10}).....	ND	.41
Pentane (C_5H_{12}).....	ND	.14
Btu value[1].....	1,014	1,057

ND Not detected.
[1]Per cubic foot at 60° F and 30 in Hg.

EXPERIMENTAL RESULTS

GAS EXPLOSIONS: BEM VERSUS LLM

A useful way to analyze gas-explosion data is to plot a wave diagram (to scale) of the static pressure-time histories at each data-gathering station with superimposed flame arrival times. Using the static pressure traces, the leading edge of the weak and strong compression and expansion waves are then sketched, and their interactions can be delineated. Wave diagrams of typical gas explosions in the BEM and the LLM are shown in figure 6. An 8.5-pct NG-air gas explosion in the BEM (15-ft zone, fig. 6*A*) is compared with an 8.6-pct CH_4-air gas explosion in the LLM (27-ft zone, fig. 6*B*). As shown in figure 6, flame acceleration and pressure rise did not become significant until the flame front had propagated approximately 15 ft in the BEM (about 0.48 s after ignition) or 30 ft (about 0.48 s after ignition) in the LLM. These observations are consistent with the high-speed film records, which indicated that the flame expanded hemispherically at a near constant rate until the flame neared the mine walls; at this stage, flame growth in the axial direction accelerated rapidly. This rapid acceleration was indicated by an abrupt change in the flame-front displacement as a function of time for both the BEM and LLM.

The maximum measured flame speeds for these two tests were about 650 ft/s. This value is considerably higher than that observed in a smooth-wall Bureau gallery (6-1/2 ft diam by 90 ft long, closed at one end) at another site, where maximum flame speeds of less than 300 ft/s were obtained for near stoichiometric CH_4-air mixtures. However, when annular rings (5 in wide) were attached to the inner surface of the first 20 ft of the smooth-wall gallery, causing a 25-pct blockage of the 33-ft^2 cross section, flame speeds and pressures increased drastically and approached those of the BEM and LLM. These annular rings resulted in the generation of large-scale turbulence, which was primarily responsible for the increase in flame acceleration. The first 50 ft of the BEM has annular rings of 4- by- 4-in wood timbers at 5 ft intervals that are used to hold the gas-zone diaphragms. Each ring provides approximately 19-pct blockage of the 54-ft^2 cross-sectional area, compared to a 13-pct blockage with similar rings of the 133-ft^2 cross section at the LLM. Rae (6), Cybulski (7), and Moen (8) have shown that flame acceleration increases with increasing blockage ratio, decreasing space between blocking rings, and increasing wall roughness.

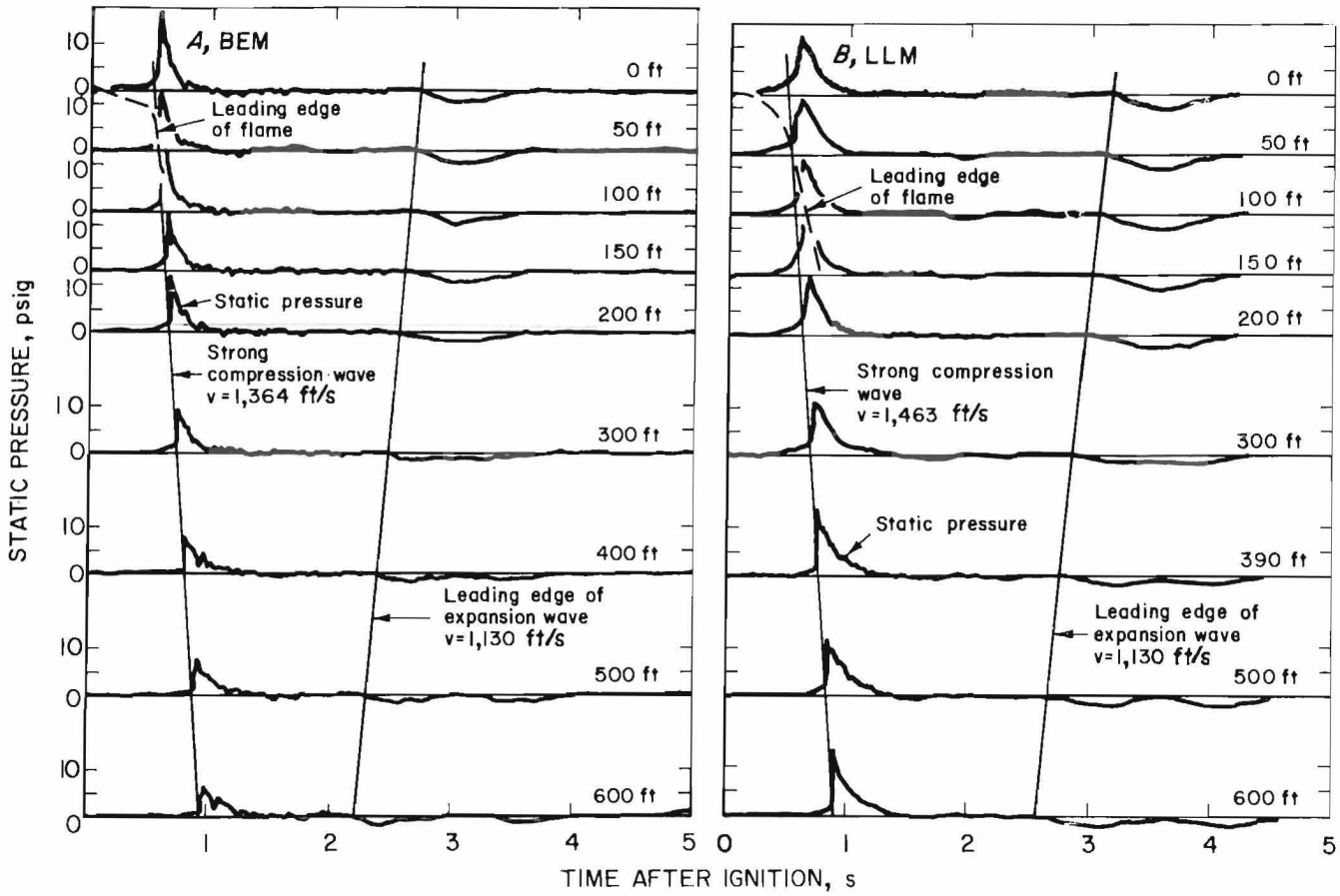

FIGURE 6.—Wave diagrams of typical gas explosion records taken from BEM and LLM. (Distances in feet indicate sensor locations, i.e., distance from face.)

The gas-explosion wave diagrams for both the LLM and the BEM show the development of a weak compression or pioneer wave that steepens into a supersonic shock wave, which propagates towards the open portal. The exiting shock wave then generates an expansion wave that propagates back toward the face at the local speed of sound. The arrival of the leading edge of the rarefaction (or expansion wave) at the face of the LLM takes about 0.32 s longer than at the BEM because of its additional 360-ft length.

Dynamics of Flame Propagation

Figure 7*A* shows the flame displacement distances as a function of time for the gas explosions conducted in D drift of the LLM for various CH_4 concentrations. Single and multiple ignition sources were used, and the flammable zone was 27 ft long.

Figure 8 shows photographs of a typical, developing explosion; the view is from the center of the entry looking toward the face. The flame expands hemispherically at a near constant rate until it nears the walls. Beyond that stage, the flame growth becomes axial and accelerates rapidly down the entry. Once it fills the cross section of the entry, flame acceleration down the entry (toward the camera) is rapid, as shown for both the 6.8-and 7.6-pct CH_4-air mixtures (fig. 7*C*). During the initial hemispherical flame growth, as measured under constant-volume combustion conditions in a 12-ft-diam sphere (9), the flame speed is on the order of 10 ft/s for stoichiometric CH_4-air mixtures and approximately 3 ft/s for the lower

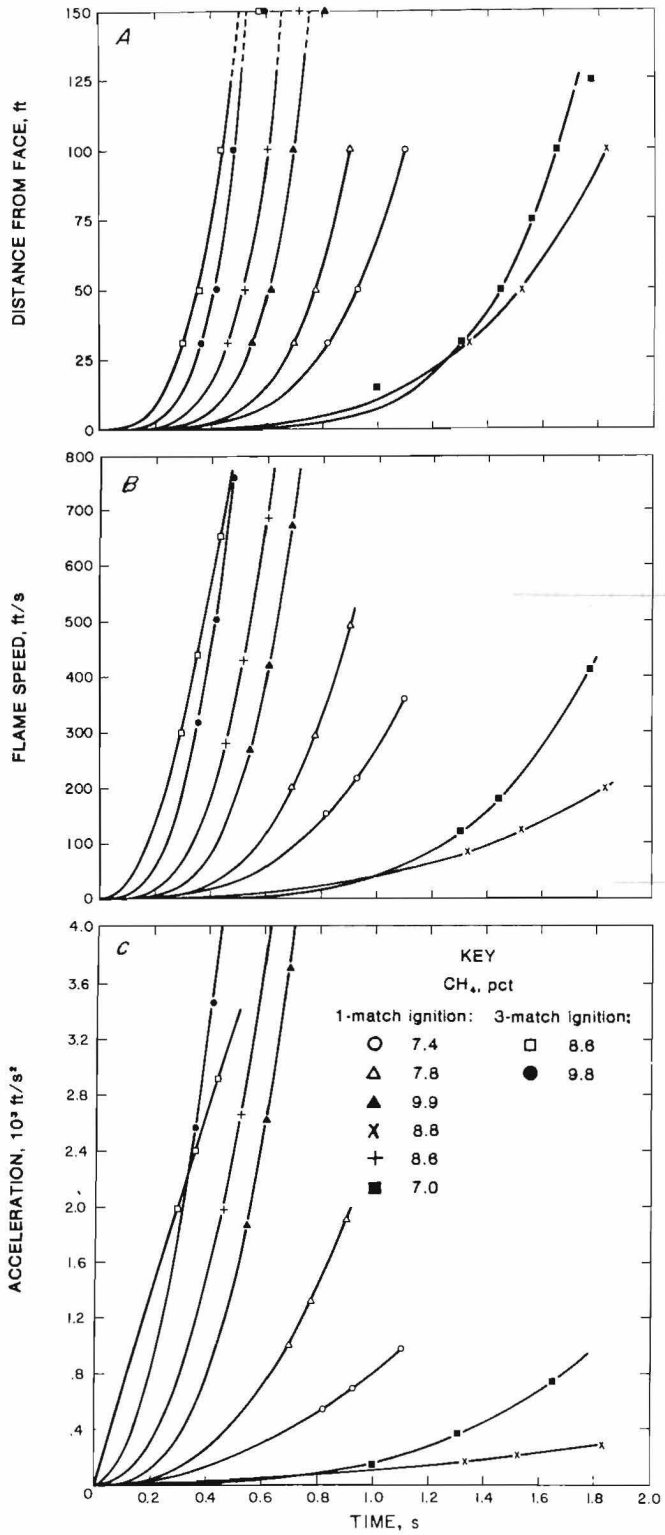

FIGURE 7.—(A) Frame displacement, (B) flame speed, and (C) flame acceleration as a function of time for gas explosions using a 27-ft gas ignitor zone at LLM.

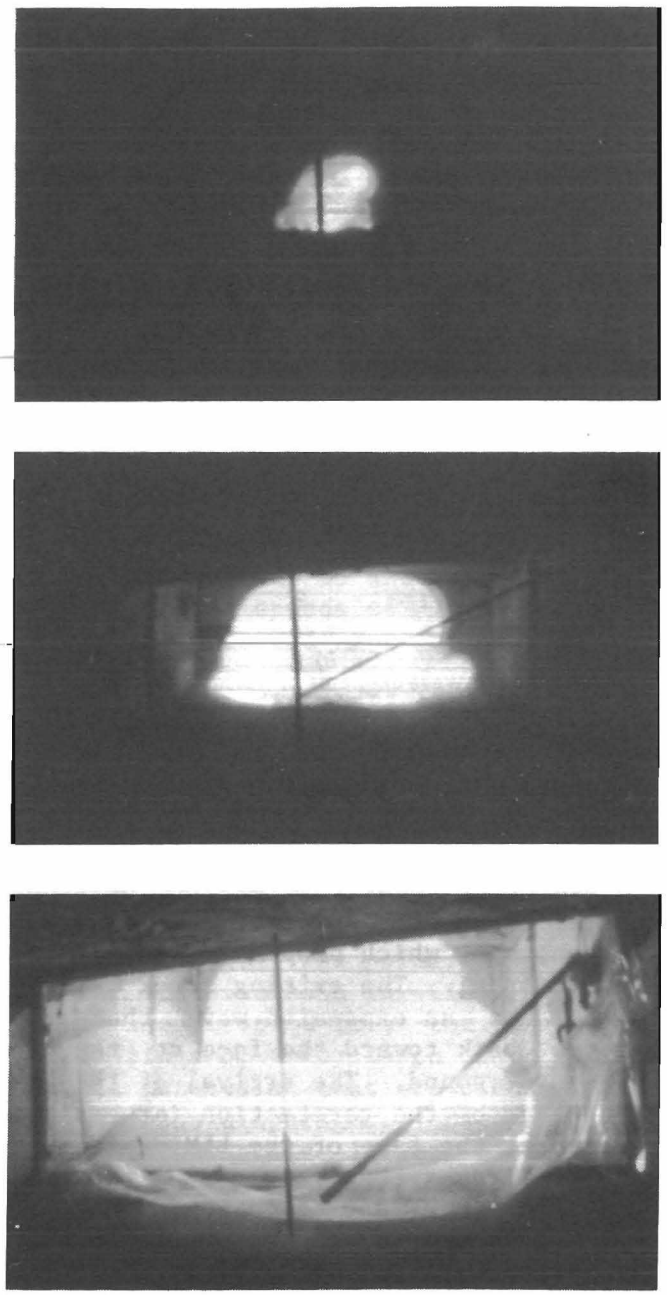

FIGURE 8.—Developing explosion from a single ignition point at LLM.

TABLE 2. - Regression coefficients of flame-displacement (D) data for various gas concentrations and ignitors at LLM, for equation $D = at^b$

CH_4, pct[1]	Matches[2]	Observation time (t), s	a	b	CH_4, pct[1]	Matches[2]	Observation time (t), s	a	b
12-ft ZONE					27-ft ZONE--Continued				
11.0	1	0.70	204.62	2.84	8.6	3	0.58	1,101.51	2.97
27-ft ZONE					9.8	3	.59	1,566.14	3.89
6.8	1	1.85	10.75	3.68	9.9	1	.80	291.55	2.82
7.0	1	1.65	7.79	5.07	40-ft ZONE				
7.4	1	1.10	77.72	4.84	7.4	1	1.16	48.11	3.95
7.4	1	1.33	31.35	5.05	9.2	1	.62	424.37	3.33
7.6	1	.91	156.11	4.49	10.1	1	.67	333.42	3.39
7.6	3	.94	151.85	6.28	10.5	1	.40	2,190.32	3.54
7.7	1	1.18	46.24	4.47	10.5	1	.73	205.96	3.04
8.6	1	.72	392.54	2.73					

NOTE: [1]Experimental variation in CH_4 analysis, ±0.4 pct.
[2]Number of matches used for ignition (at face).

explosion limit mixtures of 5.5- to 6-pct CH_4-air. However, in the mine, once the flame reaches the roof and ribs, the axial flow induces strong turbulence, and the surface area of the flame increases rapidly, resulting in an increasing rate of consumption of the unburned mixture. When the flame fills the cross section of the mine, it has displaced about 1 diam, or 20 ft of entry. The leading edge of the flame then accelerates to an average velocity of about 500 ft/s between 50 and 100 ft from the face.

The total time required to arrive at the 50-ft station varies considerably with different mixtures; this is associated mainly with the initial hemispherical growth stage. The flame data in figure 7*A* can be fitted empirically to the following equation:

$$D = at^b, \qquad (1)$$

where D is the flame-front displacement from the closed end (in feet) and t is the time (in seconds) after ignition. The regression coefficients a and b are shown in table 2. The regression coefficient a generally increases in value as the percentage of CH_4 is increased from a fuel-lean mixture. The a value peaks at an approximately stoichiometric mixture and decreases as a fuel-rich condition exists. The coefficient b shows a general decrease in value as the percentage of CH_4 is increased from a fuel-lean mixture. The b value reaches its minimum at a stoichiometric mixture and increases as a fuel-rich mixture is approached.

For CH_4-air mixtures greater than 7.4 pct, the flame propagated beyond the 100-ft station, while at lower concentrations (6.8 pct), the flame propagated (more slowly) only to the 100-ft station. A comparison of pressure histories for 1-match versus 3-match ignitions is also shown in figure 7*A*. In all cases, the 3-match ignitions (8.6- and 9.8-pct CH_4-air) showed earlier flame arrival times at the 100-ft station, and the 8.6-pct CH_4-air mixture ignited with 3 matches showed the most rapid flame velocity.

Once the flame-displacement data were fit to equation 1, the flame speed could be obtained by taking the first derivative with respect to time $\left(\frac{dD}{dt}\right)$, which gives

$$D = at^b,$$

first derivative of D is,

$$\frac{dD}{dt} = (b)(a)t^{b-1} \qquad (2)$$

where $\frac{dD}{dt}$ is equal to S_f, the axial flame speed relative to the stationary observer. Figure 7*B* shows the respective flame speeds for CH_4-air explosions in the LLM. The flame speeds at the 100-ft station ranged from a minimum of 200 ft/s for 6.8-pct CH_4-air ignited with 1 match to a maximum of about 750 ft/s for 8.6-pct CH_4-air and 9.8-pct CH_4-air ignited with 3 matches. All axial flame speeds shown were much greater than the laminar flame speed measured during constant-volume, spherical explosions (9). The typical burning velocity of stoichiometric CH_4-air is about 1.5 ft/s, and its expansion ratio (e_u/e_b) is 7.5 at constant pressure (1 atm). In laminar combustion (uniform expansion), the flame speed is equal to the product of the burning velocity and expansion ratio, so that

$$s_f = (e_u/e_b)s_u = (7.5)(1.5 \text{ ft/s})$$
$$\approx 11 \text{ ft/s}) \qquad (3)$$

A flame speed of 11 ft/s is measured only during the initial (radial or hemispherical) flame displacement; however, this rate increases very rapidly as the flame contacts the ribs and roof and the propagation becomes axial and turbulent.

Further characterizing the flame is the second derivative, flame acceleration as a function of time, as shown in figure 7*C*. Consistent with the previous results, the flame acceleration of the 9.8-pct CH_4-air mixture ignited with 3 matches was over 4,400 ft/s^2 at the 100-ft station, compared with 3,600 ft/s^2 for a similar mixture ignited with 1 match. The slowest flame acceleration was found for a 6.8-pct CH_4-air mixture with 1-match ignition and was about 300 ft/s^2 at 1.8 s after ignition at the 100-ft station.

Flame Speed

Figure 9*A* shows the flame displacements as a function of distance for gas explosions conducted in the BEM and LLM single entries. The BEM tests with 8.5- and 7.0-pct NG-air mixtures within a 15-ft gas zone resulted in the flame traveling a maximum of 50 ft from the face. The near stiochiometric 9.9-pct CH_4-air mixture and the 6.8-pct CH_4-air mixture were contained within a 27-ft zone of D drift at the LLM. The 8.5-pct BEM gas, as mentioned earlier, was near stoichiometric for the NG composition. The 9.9-pct CH_4-air mixture at LLM, which was slightly

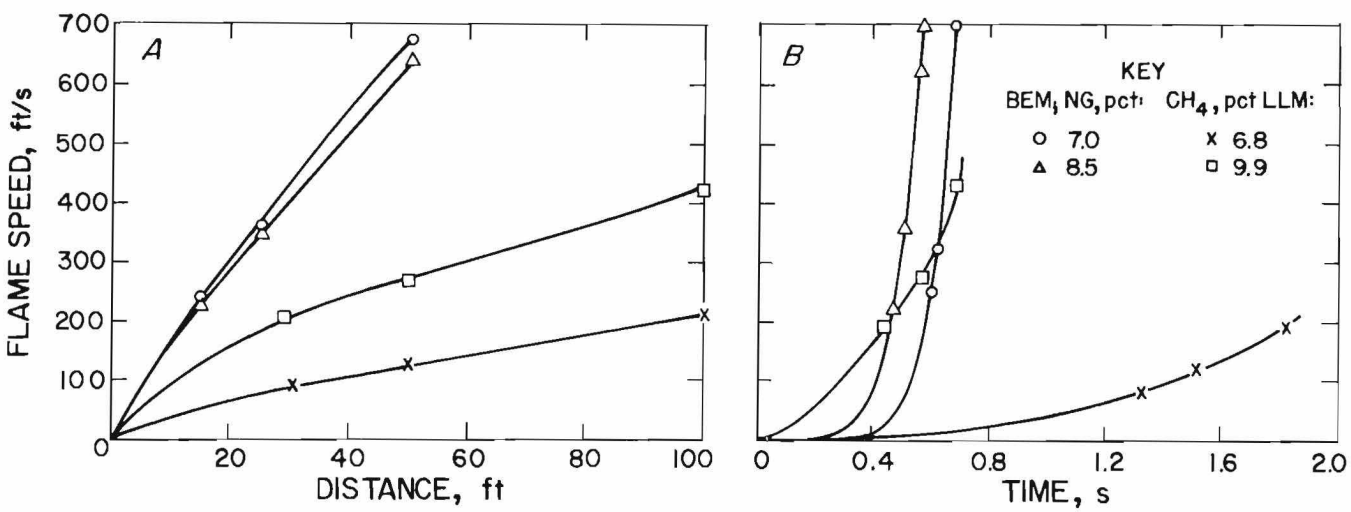

FIGURE 9.—Flame speed as a function of (A) distance and (B) time for various single-entry gas explosions at BEM and LLM.

above the stoichiometric value (9.48 pct), could thus be expected to show similar flame speeds with distance if the influence of wall roughness was the same in both entries. The two flame speed histories were very similar, as shown in figure 9*A*. However, in the case of the 6.8-pct CH_4-air mixture at the LLM, the flame arrived at the 30-ft station about 0.7 s later than the flame for the 7.0 pct NG-air mixture in the smaller BEM entry. The flame speed at the 30-ft station was about 90 ft/s at the LLM, compared to about 400 ft/s at the BEM. These differences in flame-displacement rates appear to be due to the higher blockage ratio at the BEM associated with the timber sets and the large number of these sets.

Flame-displacement data versus time were fit to the power curve as before and the flame speeds were calculated and displayed (fig. 9*B*). Comparing the flame speeds for the 9.9-pct CH_4-air mixture at the LLM with the 8.5 pct NG-air mixture at the BEM shows that after two entry widths of flame propagation, the flame speeds at the LLM and BEM were comparable. However, at farther distances, and in all other tests with comparable gas concentrations, the flame speeds were faster at the BEM than at the LLM. This was due to the internal structures attached to the rib, roof, and floor surfaces at the BEM. The internal structure at the BEM consists of a 4- by- 4-in timber supports attached to the entire entry perimeter. There are 10 such structures spaced at 5-ft intervals from the face, with the last one at the 50-ft station. They are used to support plastic diaphragms to isolate various lengths of the flammable gas zone. Each support corresponds to a blockage ratio of 19 pct. Beyond the 50-ft station at the BEM, there are steel shelves across the entry 10 to 15 in from the roof. They are spaced at 10 ft intervals, to about 400 ft.

The only internal structures at the LLM are three 4- by- 4-in timber supports. As at the BEM, the timbers are used to support plastic diaphragms and are located at 12, 27, and 40 ft from the face. Because the LLM entries are larger than those in the BEM, they represent a smaller blockage ratio of 13 pct; and there are only 3, compared with 10 at the BEM. There are no steel shelves at the LLM; however, there are several platform stations.

Pressure History

Wave Diagram

The 100-ft station was chosen to compare pressure histories for explosions of 27-ft zones of CH_4-air in the LLM's D drift. The various pressure histories at the 100-ft station are shown as a function of time in figure 10. The 6.8-pct CH_4-air mixture had the slowest flame velocities (fig. 7*B*) and also gave rise to the lowest maximum pressure of 3 psi at 1.7 s after ignition. A stiochiometric CH_4-air mixture, which burned about twice as fast as the 6.8-pct CH_4-air mixture, resulted in a peak pressure of 6 psi at 0.85 s. The 8.6-pct (±0.4 pct) CH_4-air mixture appears to have had the fastest burning rate and the fastest pressure rise. As shown in figure 7*C*, this mixture also had the highest flame acceleration rates. As shown in figure 10, the 9.9-pct CH_4-air (slightly fuel-rich) mixture burned slightly slower than the 8.6 pct mixture, but faster than the 7.6-pct CH_4-air mixture. Typically, the maximum explosion pressure measured at the BEM is associated with a 10-pct NG-air mixture with single-spark ignition. The differences in the concentrations at which maximum flame speed and pressure rise occurred in the LLM and the BEM were possibly due to the types of ignition sources used in each mine. The single-spark ignition at the BEM provided a well-formed, small ignition kernel; whereas, the electric matches used at the LLM resulted in multiple ignition sources being thrown out by the exploding match. This effect can be seen in the top photo in figure 11, in which the match is on the right. These multiple sources caused enhanced fireball development within the first 15 ft of the face. The variability from match to match and the reproducibility of gas concentration (±0.4 pct CH_4) may be part of the reason why the

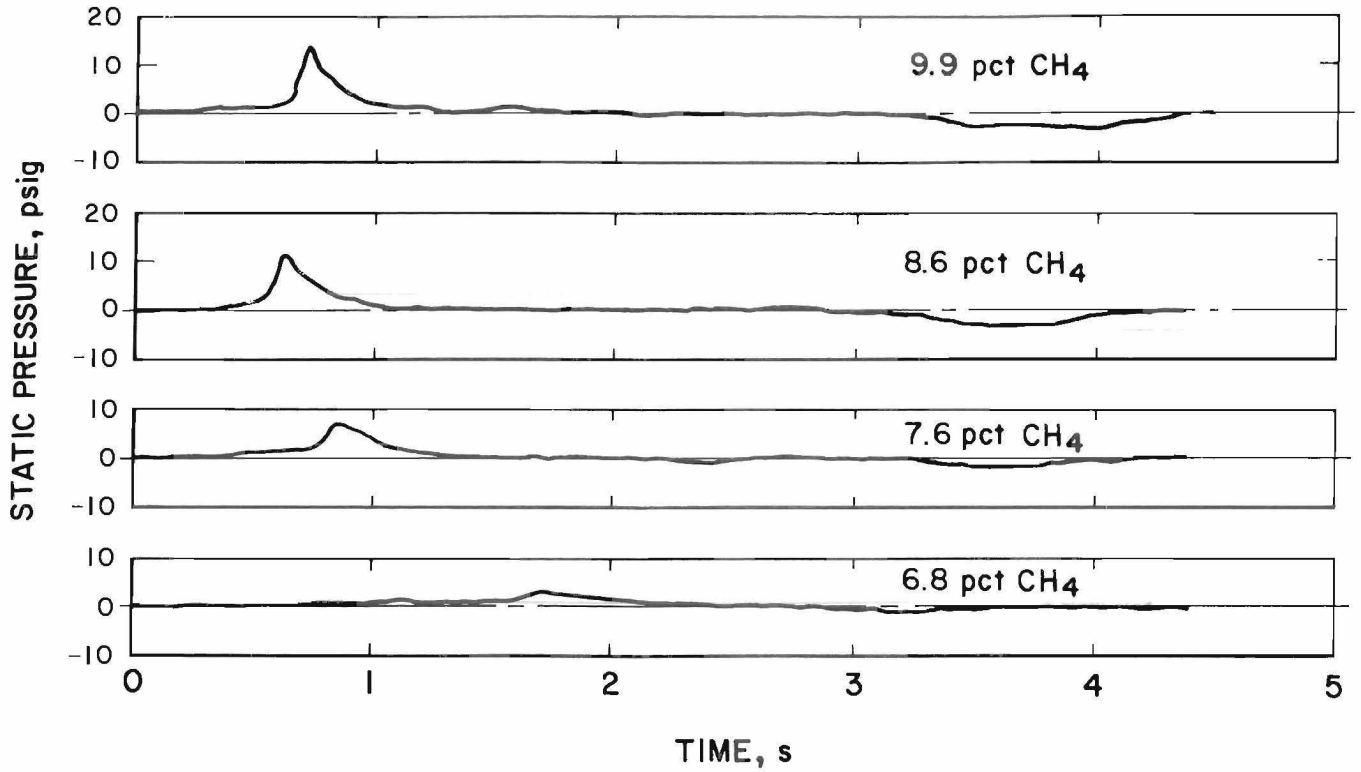

FIGURE 10.—Static pressure histories at 100 ft from the face for various CH_4-air mixtures at LLM.

8.6-pct CH_4-air gas explosion developed faster than the 9.9-pct CH_4-air explosion in the early stages of flame development. However, in the later stages, the flame acceleration of the 9.9-pct CH_4-air mixture exceeded that of the 8.6-pct CH_4-air mixture (fig. 7*C*). At the LLM, a near-limit mixture, or a mixture of CH_4-air at its lower explosive concentration, containing 5.4 pct CH_4-air was ignited with one electric match, and the maximum pressure measured was less than 1 psi, and the flame developed very slowly. High-speed photographs showed a bouyant, pale-blue fireball moving towards the roof, spreading out, and then propagating downward towards the floor as a relatively flat flame front.

Impulse

The pressure impulse is an important measure of the damaging potential of the explosion pressure pulse. The impulse is the time integral of the pressure (p) profile, $\int p(t)dt$, or the area under the pressure-time curve. The destructive forces of the explosion blast wave depend on both the maximum peak overpressure and the impulse. Typical maximum face overpressures, impulses, and heat release for the flammable gas-air mixtures used in this study are shown in tables 3 and 4 for the BEM and the LLM. Increasing gas concentrations increase heat release and generally increase the maximum overpressures and impulse. However, to obtain comparable impulses, the LLM requires about three times the heat release as the BEM. The maximum overpressure and the impulse depend not only on the total energy released, but also on the rate at which it is released.

TABLE 3. - Maximum overpressures, impulses, and energy-release data from various NG explosions within the BEM (15-ft gas zones)

NG.....pct..	7.0	8.5
Max overpressure.....psig..	8.7	16.6
Impulse.....lbf·s/ft^2..	187	289
Heat release.....10^3 Btu..	60	73

Shown in figure 12 are the impulses for tests with 7.6- and 6.8-pct CH_4-air mixtures at the LLM and tests with 8.5 and 7.0-pct NG-air mixtures at the BEM. The LLM used 27-ft test zones, and the BEM used 15-ft zones. The measured impulses for the LLM and BEM decreased in value for the first 150 to 200 ft from the face and then remained constant throughout the downstream stations. The 8.5-pct NG-air explosion at the BEM generated a 16-psig face pressure, which decayed to 5.5 psig 600 ft from the face. Although the peak overpressure decreased, the impulse remained relatively constant from 200 to 600 ft from the face. However, the LLM pressure remained relatively unchanged in shape between 200 and 600 ft; whereas, the BEM pressure decayed while the pulse became wider.

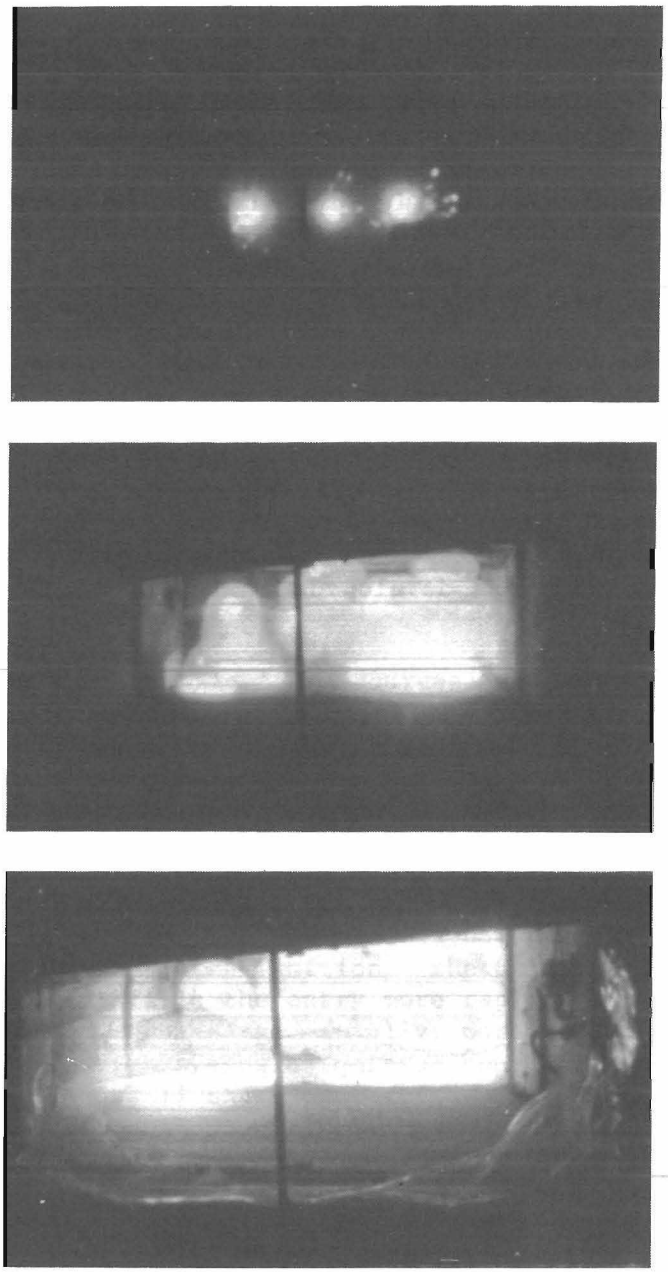

FIGURE 11.—Explosion development from multiple ignition points at LLM.

TABLE 4. - Maximum overpressures, impulses, and energy-release data from various CH_4 explosions within the LLM (27-ft gas zones)

CH_4.....pct..	6.8	7.0	7.6	8.6	9.8
Max overpressure psig..	3.9	6.2	7.4	12.4	18.3
Impulse $lbf \cdot s/ft^2$..	250	366	331	446	471
Heat release 10^3 Btu..	241	249	268	306	348

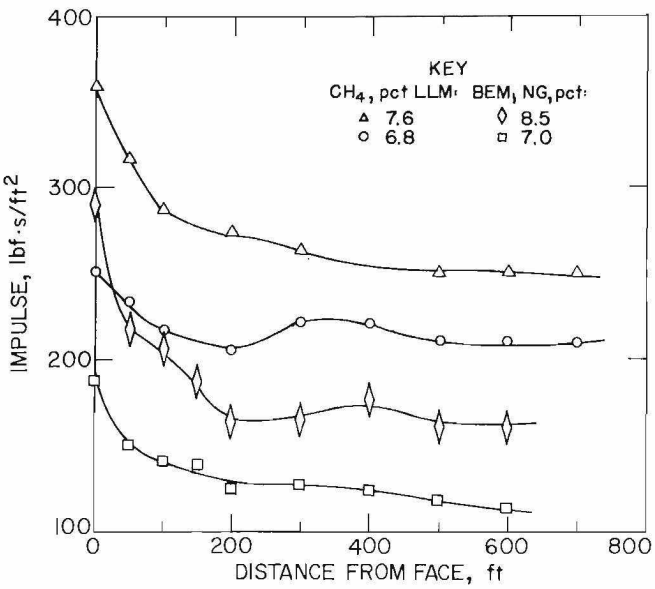

FIGURE 12.—Pressure impulse as a function of distance from the face for various flammable gas-air mixtures for BEM and LLM explosions.

Pressure Decay

Once all the fuel is consumed and the flame has accelerated to its maximum velocity, the flame dies out, and the pressure pulse ceases to grow, but the pressure disturbance continues to propagate toward the open end. The pressure pulse will interact with the mine surfaces and start to dissipate. The rougher the wall, the greater the interaction and the more rapid the dissipation of the pressure pulse. Both the BEM and LLM have about the same local rib and roof roughness. The influence of this roughness on the aerodynamic flow field is greater in the smaller entry (BEM) than in the larger entry (LLM). The perimeter surface-to-volume ratio for each 1 ft of entry at the BEM and the LLM can be compared. The ratios are 30 ft^2/54 ft^3 = 0.55 at the BEM and 52 ft^2/133 ft^3 = 0.39 at the LLM. Thus, the surface-to-volume ratio is about 40 pct larger at the BEM than at the LLM.

Figures 13 and 14 show a comparison of the maximum pressures with distance from the face (closed end) at the BEM and the LLM, respectively. A near-stoichimetric NG-air mixture (8.5 pct) in a 15-ft zone at the BEM showed a maximum face pressure of 16 psig, which decayed to approximately 5.5 psig 600 ft from the face; whereas, the 6.5-pct NG-air mixture decayed to about 50 pct of its face value, to 3.5 psig, at 600 ft (fig. 13).

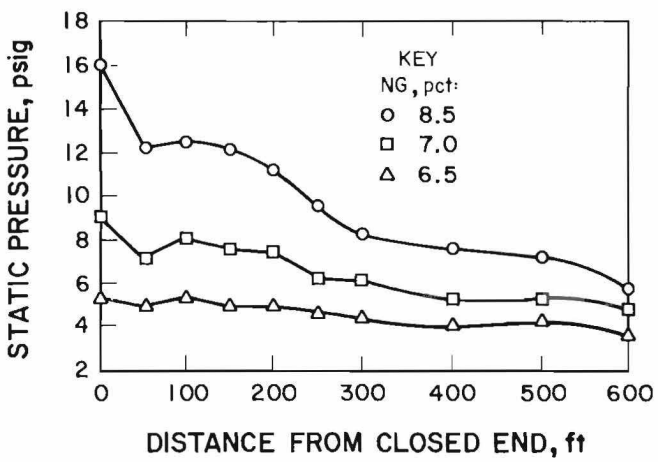

FIGURE 13.—Peak static pressures as a function of distance for three NG-air mixtures in BEM.

The LLM, with its near-stoichiometric CH_4-air mixture, gave a face pressure of 14.5 psig, which decayed to 11 psig at 600 ft (fig. 14). In all tests shown, there was very little decay with distance at the LLM as compared with the BEM results.

Also shown in figure 14 (shaded areas) is the region where a shock was riding on the leading edge of the pressure pulse. The top of the shaded area indicates the peak pressure of the shock, and the lower portion of the shaded area indicates the maximum pressure immediately behind the shock. The slowest burning mixture of 6.8-pct CH_4-air did not develop into a shock within the first 750 ft of propagation; whereas, the faster burning near-stoichiometric 9.9-pct CH_4-air showed shock development at approximately 200 ft. The magnitude of the shock for the 8.6-pct CH_4-air increased slightly between 300 and 600 ft, from 14 to 15 psig. The faster the initial flame acceleration at the face, the closer to the face the shock developed.

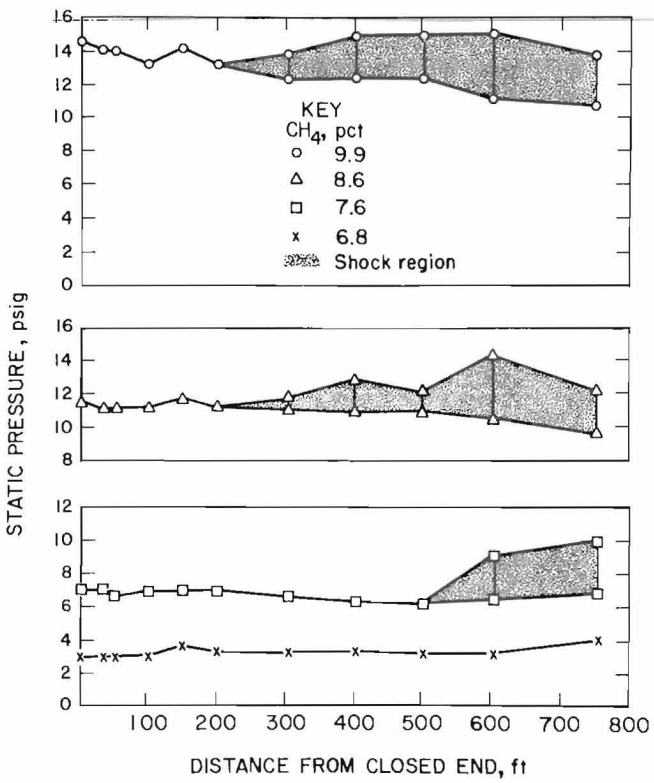

FIGURE 14.—Peak pressures as a function of distance for four CH_4-air mixtures at LLM.

Wall roughness not only dissipated the pressure pulse, it also caused a higher initial flame acceleration in the smaller entry. The turbulence levels in the BEM explosions were also higher at the instant the flame consumed the last volume of flammable gas. Higher turbulance in the unburned gas can also cause more rapid dissipation of the pressure pulse, quite independent of the surface-to-volume ratio.

The pressure-decay profiles in figures 13 and 14 show that the peak pressure at the BEM decayed rapidly as it moved down the entry; whereas, at the LLM, there was little decay for the first 600 ft. As shown in figure 10*B*, the corresponding flame speeds at the BEM were considerably faster than those at the LLM. Flame acceleration was more rapid at the BEM because of the stronger wall interactions, higher blockage ratio, higher surface-to-volume-ratio, and the larger number of blockages and their periodicity. For the same reasons, the pressure pulse decayed more rapidly at BEM once propagation ceased.

Ignition Sources

Multiple Ignitions

With the single-ignition source (electrical match) at the face, the flame expands hemispherically until it fills the entry and then starts to accelerate rapidly toward the open end. However, with a three-match ignition, the flame initially fills the entry more rapidly. It then accelerates axially more rapidly than with a single-ignition source.

Figure 11 shows photographs of a developing explosion resulting from a three-match ignition. Figure 15 shows the 100-ft pressure histories of 8.6- and 9.8-pct CH_4-air mixtures at the LLM ignited with one and three matches. The three-match ignition (8.6-pct CH_4-air) caused the pressure to peak about 0.2 s sooner than the one-match ignition (8.6-pct CH_4-air). Also, the rapid flame acceleration in the three-match tests showed the steepening of the pressure curve leading to shock formation much sooner than in the one-match tests. The same relative effect for the 9.8 pct CH_4-air mixture is shown, with the triple-ignition pressure peaking 0.2 s sooner and shock formation occurring the top of the pressure peak. The maximum pressures are about the same for both mixtures with both one- and three-match ignitions. Multiple ignitions have the effect of accelerating the flame earlier, resulting in earlier peaking of the pressures, but without significant changes in the maximum pressures or the impulse of the explosion.

Location of Ignition Source

Figure 16 shows the measured pressure histories at the 100-ft station from explosions in D drift for 7.6-pct CH_4-air contained within the first 27 ft of the face. The upper trace is for ignition of the CH_4 zone at a distance of 0.5 ft from the face (face ignition). The middle curve is for ignition in the same zone, but at 13.5 ft from the face (central ignition). The bottom trace is for ignition at the plastic diaphragm, at the open end of the flammable zone, 27 ft from the face (diaphragm ignition). Differences in peak pressures are apparent in the arrival times, and widths of the pressure-time profiles.

In the face-ignition test, the arrival time for the pressure peak was almost coincident with the arrival of the flame front. In this case, the turbulence increased continuously in the unburned gas, which expanded outward. Face ignition caused a continuous acceleration of the flame as it consumed the turbulent unburned gas ahead of it. The initial unburned gas zone was continuously displaced outward as burned gas accumulated behind it. The flame front overtook and consumed the unburned gas at its turbulent burning velocity. The leading edge of the unburned gas zone was pushed by the expansion of the burned gas to about 100 ft from the face by the time it was completely consumed by the combustion front. The measured peak overpressure was 7 psig when the flame reached 100 ft, at about 0.9 s, and the instantaneous

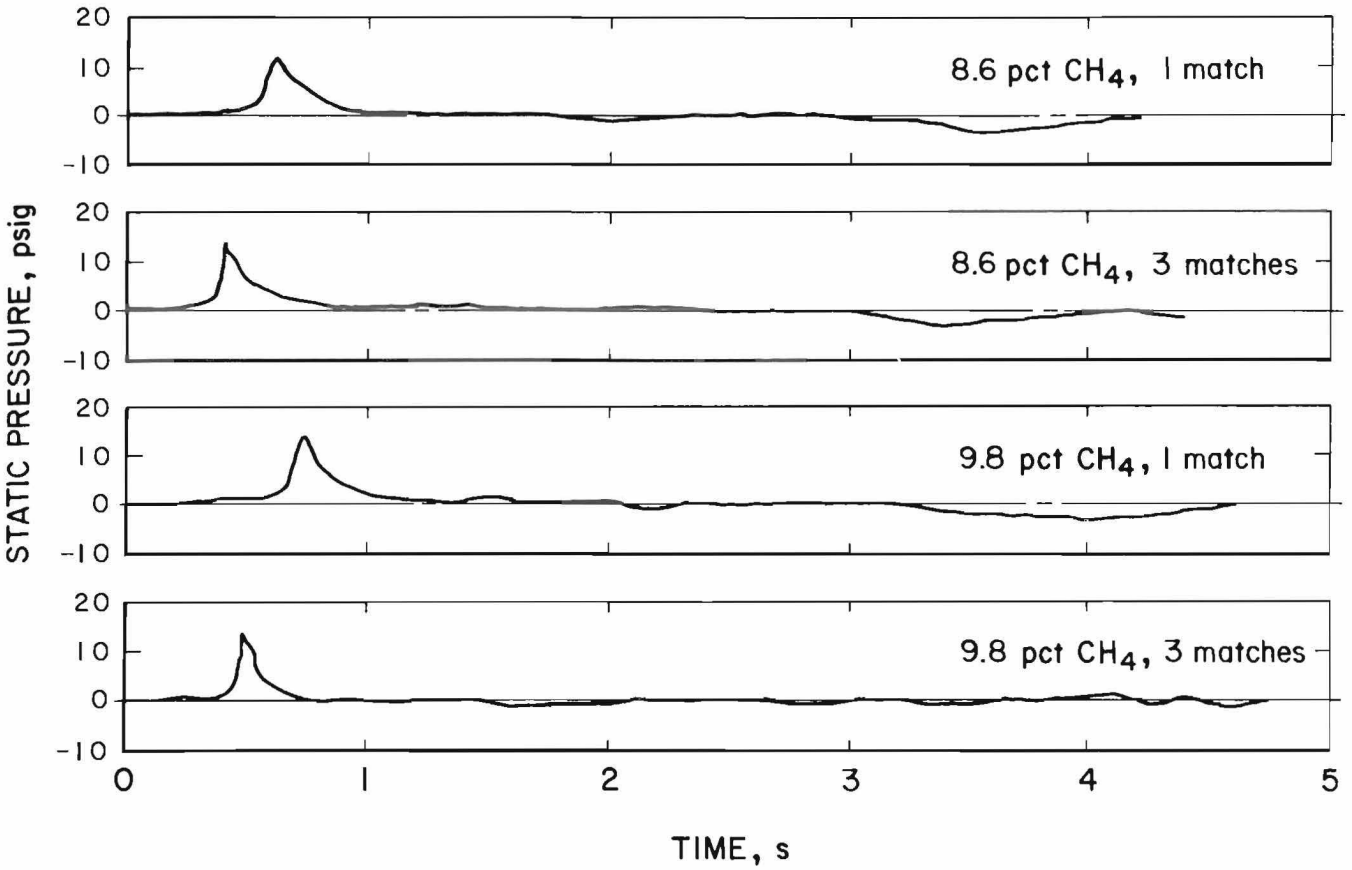

FIGURE 15.—Static pressure histories at the 100-ft station for single and triple ignitions for 8.6- and 9.8-pct CH_4-air explosions at LLM.

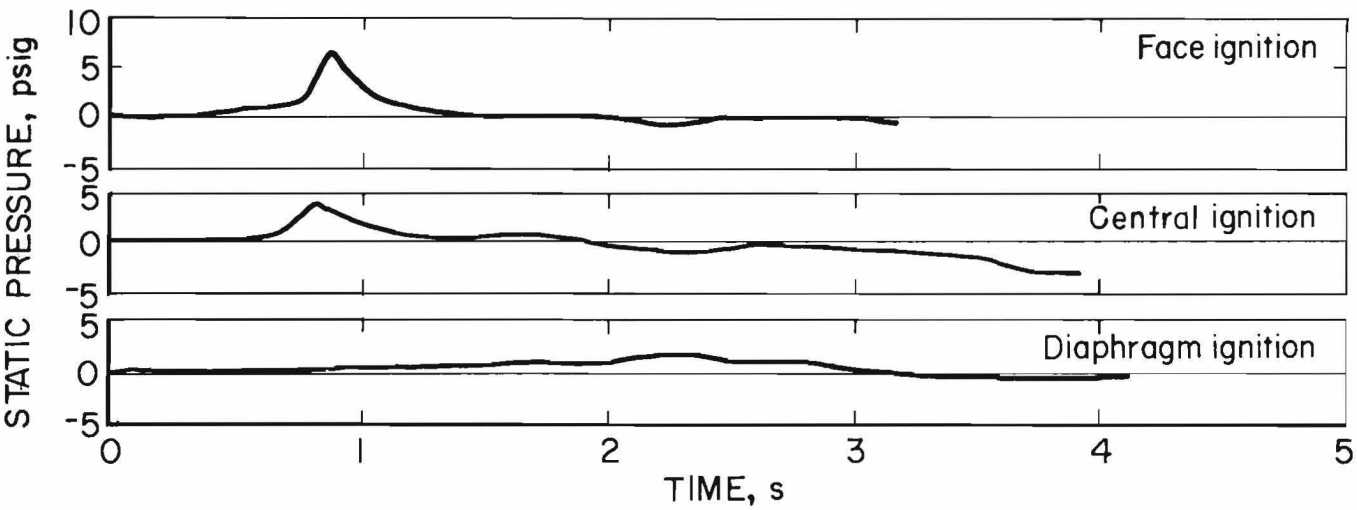

FIGURE 16.—Comparisons of pressure histories from 100-ft station for 7.6-pct CH_4-air gas explosions initiated at the face, central, and diaphragm positions in D-drift.

maximum flame speed at that distance was about 500 ft/s. But since the flame traveled some 100 ft in 0.9 s, its average velocity during that interval was 110 ft/s.

With central ignition, the flame propagated both toward and away from the face. The combustion wave that propagated toward the face consumed about half of the flammable volume, and the wave that propagated toward the open end consumed the other half. Even though each wave traveled only half the distance traveled in the face-ignition test, the time of peak pressure for central ignition was about the same as for face ignition. The flame-travel distance toward the open end was about 86 ft, and it took about 0.55 s for the pressure peak to reach the 100-ft station, resulting in an average speed of 102 ft/s. This speed, comparable to the 110-ft/s average speed for face ignition, suggests that the turbulent acceleration associated with the outby flame propagation was essentially the same in both cases. However, for central ignition, the peak pressure was only 4 psig; whereas, for face ignition, it was 7 psig, (fig. 16). The outward-traveling flame (toward the open end) propagated much faster than the inward-traveling flame (toward the face). Accordingly, the pressure peak associated with the outward-traveling turbulent flame arrived at the 100-ft station long before the inward-traveling flame had consumed its half of the flammable volume. This occurred because the inward-traveling flame propagated through the gas that was confined by the face, and there was little or no opportunity for motion of that gas or, consequently, any resultant turbulent acceleration. With central ignition, the inward flame consumed its half of the flammable volume considerably later than the outby flame consumed its half, and the peak pressure was considerably lower. The pressure decay profile for central ignition, which extended out to about 2 s (fig. 16), reflected the slower speed of the inward-traveling flame. The inward flame took about 2 s to travel 13.5 ft, which corresponds to a speed of about 7 ft/s. The inward flame speed remained fairly constant at 7 ft/s; whereas, the outward flame velocity accelerated continuously, so that its maximum speed as it consumed the last fraction of its flammable volume was probably about five faster than its average speed.

Ignition of the flammable volume at its open end near the plastic diaphragm yielded a peak pressure of only 2 psig, and it took 2.3 s for the flame to consume the flammable volume. There was only slow propagation toward the face, and the absence of significant turbulent acceleration of the flame was reflected in a very slow growth of the pressure profile (fig. 16).

The data in figure 16 show clearly that the location of the ignition source within the flammable volume determines the intensity of the resulting gas explosion. The intensity or pressure rise increases the closer the ignition is to the closed end, because a larger fraction of the flammable volume is being involved in tubulent burning.

Other Explosion Characteristics

Wind Velocity

During a gas explosion in the single entry at the LLM, the heated gases expand to about five times their initial volume. As a result, the air and unburned gas are pushed ahead of the flame, generating a wind ahead of the flame front directed toward the open end. As the flame accelerates, so does the unburned mixture ahead of the flame. The rate at which the flame overtakes and consumes the receding unburned mixture is referred to as the burning velocity. The flame propagates into the flow field set up by its own pistonlike motion.

Typical wind velocities ahead of the flame at the 50-, 100-, and 150-ft stations for explosions at the LLM are shown in figure 17. At the 50-ft station, the air velocity increased to about 40 ft/s in about 0.3 s. At the 150-ft station,

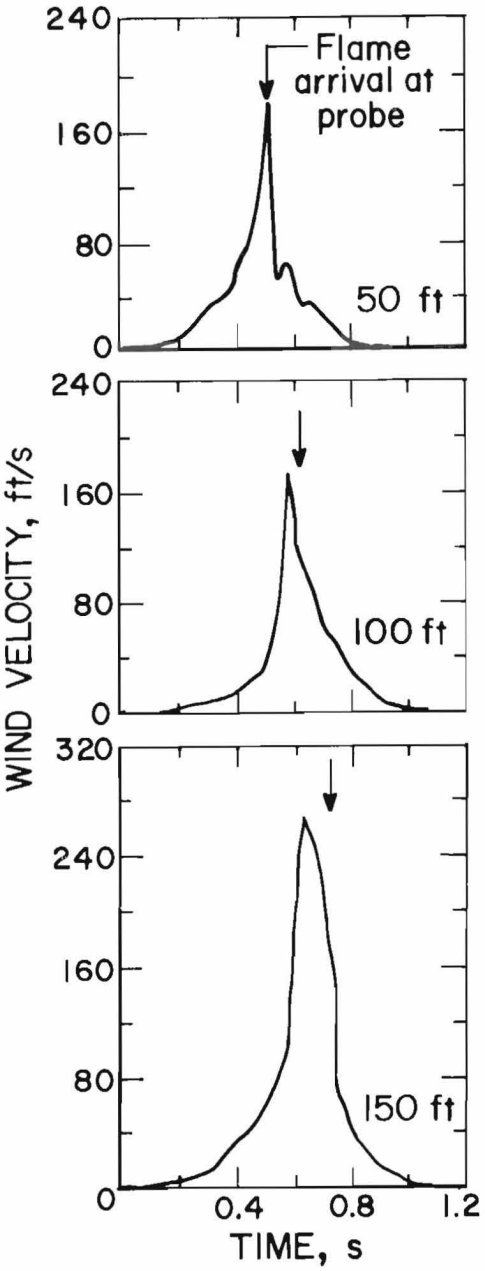

FIGURE 17.—Typical wind-velocity data at three stations for a CH_4-air gas explosion at LLM. (Distances in feet indicate sensor locations, i.e., distance from ignition point.)

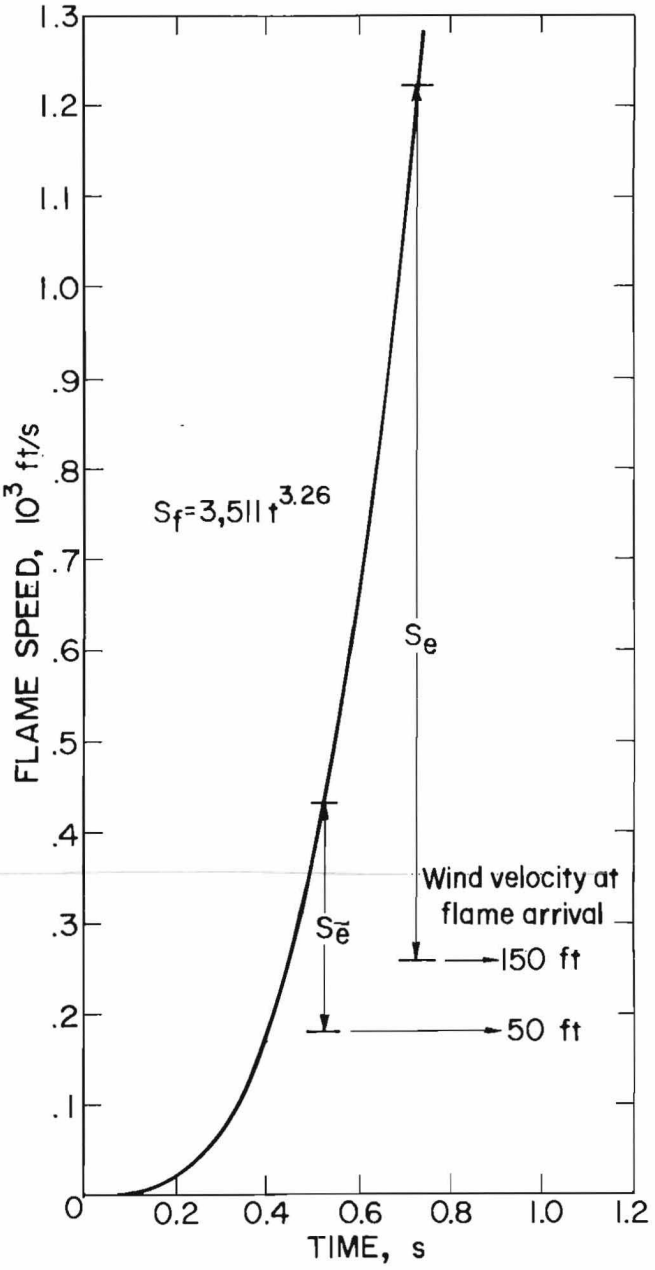

FIGURE 18.—Typical flame speed and wind-velocity data at the leading edge of the flame front for a CH_4-air gas explosion at LLM.

it increased to 250 ft/s in about 0.5 s, showing very rapid acceleration over a 100-ft interval. As soon as the flame front arrived at a probe, the air velocity rapidly fell to zero in the burned gases behind the flame front. The data also show that the air velocity reached a maximum value of 260 ft/s at the 150-ft measuring station just before flame arrival. The difference between the flame speed (S_f) at the station and the wind velocity (v) at the time of flame arrival is equal to the effective (or turbulent) burning velocity (S_e), as shown in the equation

$$S_e = S_f - v. \qquad (4)$$

The flame speed and wind velocity at the leading edge of the flame are shown in figure 18. When the flame arrived at the 50-ft station, the flame speed was about 425 ft/s, and the maximum air velocity was about 180 ft/s, giving an effective burning velocity of about 245 ft/s. About 0.2 s later, at the 150-ft station, the measured flame speed was about 1,200 ft/s, with a corresponding wind velocity of 280 ft/s. The effective burning velocity had increased to 900 ft/s, reflecting a 3.5-fold increase between the two stations. As can be seen from calculation, the effective burning velocity was quite high and increased with propagation distance until the unburned fuel mixture was consumed. This rapid acceleration would continue as long as there was unburned fuel ahead of the flame, until a detonation wave developed.

Heat Flux

As Moen (8) has idealized, a one-dimensional flame with a burning velocity, S_u, can be defined in terms of the heat release per unit of projected area (q) by the relation

$$\dot{q} = Q\int_{\text{flame surface}} S_u dA \qquad (5)$$

where A is the unit of projected area, S_u is the burning velocity component normal to the flame surface, and Q is the heat content per unit volume of mixture. For flame propagation perpendicular to the flame surface area, (A_s),

$$\dot{q} = QS_uA_s. \qquad (6)$$

As shown previously, the effective burning velocity and heat-release rate increase very rapidly with time and distance from the face. These increases were associated with the increase in flame surface area resulting from turbulence. The hot combustion products transfer heat to the cold mine surfaces and cool. Heat-flux measurements at the rib and 50, 152, and 390 ft from the face, are shown in figure 19 for a 10-pct CH_4-air mixture at the LLM. Peak wall heat transfer occurred at the flame front and decreased rapidly after its passage. The instant the flame arrived at the station, the wall heat loss was at a maximum, at about 25 cal/cm^2·s. At about 0.5 s after the passage of flame, the gas combustion products had cooled to the point where the heat flux had decreased to about 2.5 cal/cm^2·s. This rapid cooling may be part of the reason why the maximum flame extension from the face was only 5.5 times the length of the initial gas zone instead of the calculated 7.5 times (1 atm) expected from the adiabatic expansion ratio. The heat-flux reading at the 390-ft sensor was due to the cooling of the residual hot gas pulse, since the flame was observed only to 200 ft.

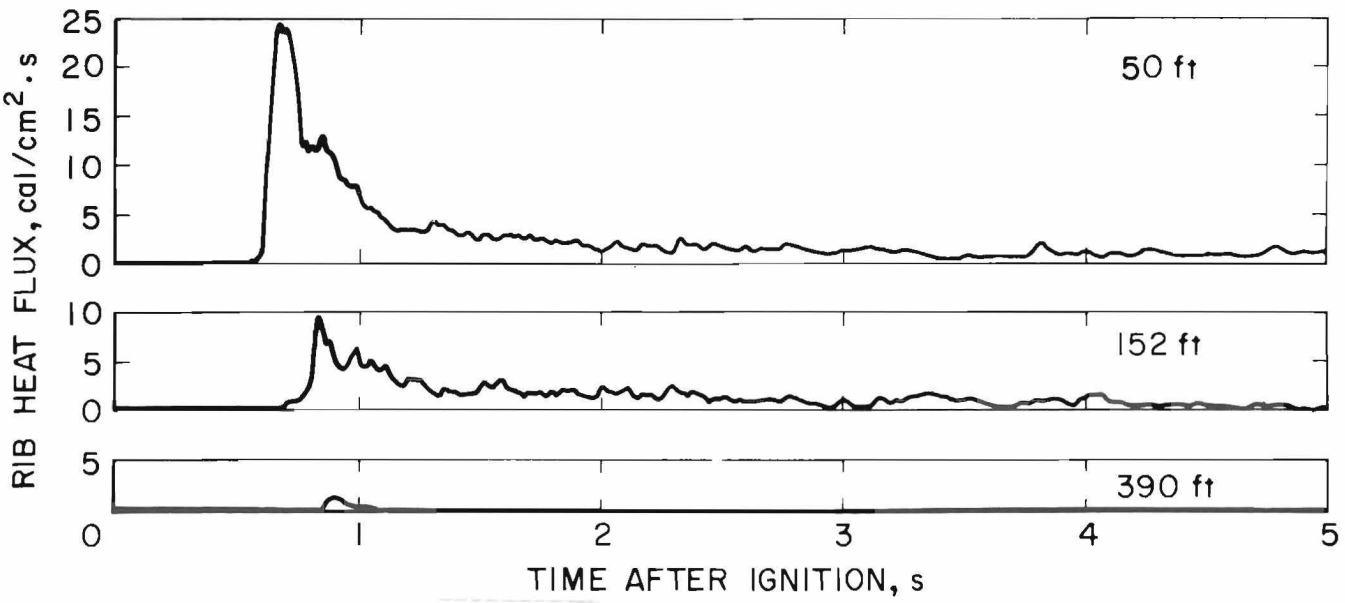

FIGURE 19.—Heat-flux measurements for a 10-pct CH_4-air gas explosion at LLM. (Distances in feet indicate sensor locations, i.e., distance from face.)

CONCLUSIONS

Flame-front displacement for the LLM and the BEM explosions can be characterized by the expression $D = at^b$, where a and b are functions of gas concentration, location of ignition source, and length of flammable volume. The flame accelerated faster in the BEM than at the LLM for all CH_4-air mixtures tested. The blockage ratio associated with timber sets appears to influence the flow field in the smaller BEM entry more than in the larger LLM entry. The higher blockage ratio at the BEM caused a greater degree of turbulence to be generated in the unburned gas ahead of the flame.

The results show that the pressure pulse decayed less rapidly in the larger LLM entry because of the larger perimeter-to-cross-sectional-area ratio. Furthermore, the greater number of periodic obstructions in the BEM and its smaller ratio of perimeter to cross-sectional area caused the pressure pulse to diminish more rapidly. The same factors that caused the higher acceleration of the flame front at the BEM appear to have been responsible for the more rapid decay of the pressure pulse at the BEM.

REFERENCES

1. Humphrey, H. B. Historical Summary of Coal-Mine Explosions in the United States, 1810-1985. BuMines B 586, 1960, 280 pp.

2. Richmond, J. K., G. C. Price, M. J. Sapko, and E. M. Kawenski. Historical Summary of Coal Mine Explosions in the United States, 1959-81. BuMines IC 8909, 1983, 53 pp.

3. Mattes, R. H., A. Bacho, and L. V. Wade. Lake Lynn Laboratory: Construction, Physical Description, and Capability. BuMines IC 8911, 1983, 40 pp.

4. Hertzberg, M., and C. D. Litton. Pneumatic Fire Detection With Tube Bundles. J. Fire Flammability, v. 9, 1978, pp. 199-216.

5. Multipoint Detection of Products of Combustion With Tube Bundles. Transit Times, Transmissions of Submicrometer Particulates, and General Applicability. BuMines RI 8171, 1976, 40 pp.

6. Rae, D. Experimental Coal Dust Explosions in the Buxton Full-Scale Surface Gallery. Part II-The Influences of Arches and Dust Barriers Pressure Release and Rocket Ignitors Strength on the Characteristics of Explosion. SMRE (London) Res. Rep. 266, 1971, 41 pp.

7. Cybulski, W. Coal Dust Explosions and Their Suppression (translated from Polish). Nat. Cent. for Sci. Tech. and Econ. Inf., Warsaw, Poland, 1975, pp. 237-250.

8. Moen, I. O. The Influence of Turbulence on Flame Propagation in Obstacle Environments. Fuel-Air Explosions. Univ. of Waterloo Press, 1982, 34 pp.

9. Sapko, M. J., A. L. Furno, and J. M. Kuchta. Flame and Pressure Development of Large-Scale CH_4-Air-N_2 Explosions. Buoyancy Effects and Venting Requirements. BuMines RI 8176, 1976, 32 pp.

U.S. GOVERNMENT PRINTING OFFICE: 1987 - 605-017/60113

INT.-BU.OF MINES,PGH.,PA. 28581